ELSEVIER

Contents lists available at ScienceDirect

Free Radical Biology and Medicine

journal homepage: www.elsevier.com/locate/freeradbiomed





Modeling the reactive oxygen species (ROS) wave in *Chlamydomonas* reinhardtii colonies

Yuanzhe Zhou^a, Yosef Fichman^b, Sicheng Zhang^a, Ron Mittler^{c,d,**}, Shi-Jie Chen^{a,e,*}

- ^a Department of Physics and Astronomy, University of Missouri, Columbia, MO, 65211, USA
- b School of Plant Sciences and Food Security, George S. Wise Faculty of Life Sciences, Tel Aviv University, Tel Aviv, 6997801, Israel
- ^c Division of Plant Science and Technology, College of Agriculture, Food and Natural Resources and Interdisciplinary Plant Group, Christopher S. Bond Life Sciences Center, University of Missouri, 1201 Rollins St, Columbia, MO, 65211, USA
- d Department of Surgery, School of Medicine, Christopher S. Bond Life Sciences Center, University of Missouri, 1201 Rollins St, Columbia, MO, 65211, USA
- e Department of Biochemistry, MU Institute for Data Science and Informatics, University of Missouri, Columbia, MO, 65211, USA

ARTICLE INFO

Keywords: Cell-to-cell signaling ROS wave ROS-Induced-ROS release Reaction-diffusion

ABSTRACT

Reactive oxygen species (ROS) play a crucial role as signaling molecules in both plant and animal cells, enabling rapid responses to various stimuli. Among the many cellular mechanisms used to generate and transduce ROS signals, ROS-induced-ROS release (RIRR) is emerging as an important pathway involved in the responses of various multicellular and unicellular organisms to environmental stresses. In RIRR, one cellular compartment, organelle, or cell generates or releases ROS, triggering an increased ROS production and release by another compartment, organelle, or cell, thereby giving rise to a fast propagating ROS wave. This RIRR-based signal relay has been demonstrated to facilitate mitochondria-to-mitochondria communication in animal cells and long-distance systemic signaling in plants in response to biotic and abiotic stresses. More recently, it has been discovered that different unicellular microorganism communities also exhibit a RIRR cell-to-cell signaling process triggered by a localized stress treatment. However, the precise mechanism underlying the propagation of the ROS signal among cells within these unicellular communities remained elusive. In this study, we employed a reaction-diffusion model incorporating the RIRR mechanism to analyze the propagation of ROS-mediated signals. By effectively balancing production and scavenging processes, our model successfully reproduces the experimental ROS signal velocities observed in unicellular green algae (Chlamydomonas reinhardtii) colonies grown on agar plates, furthering our understanding of intercellular ROS communication.

1. Introduction

The diffusion of a single signaling molecule, in its prototypical form, is a relatively slow process. It is insufficient to explain the rapid signaling rates observed in diverse biological processes [1–13], where groups of cells or subcellular components collectively engage in signaling reactions to generate rapidly propagating signaling waves. In these processes, diffusible molecules released by individual cells or subcellular components activate neighboring cells, giving rise to self-propagating waves. Throughout the years, numerous diffusion-reaction models [14–34] have been proposed to describe the propagation of traveling waves or signals that govern a wide range of

intracellular and cell-to-cell signaling processes. Examples include the systemic response of plants to salt stress [14], pattern formation in *Dictyostelium* [15–18], bacterial quorum sensing [19–22], mitochondrial oscillations [23,24], and calcium waves [25–32]. While computational approaches have been employed to study reactive oxygen species (ROS) production and its regulation in different signaling pathways [14,23,24, 35,36], modeling ROS-induced-ROS-release (RIRR) propagation in cell-to-cell signaling is still new. The computational model proposed here expands beyond plant cells [14] and delves into microorganism communities, where the ROS wave velocity is influenced by population density and other parameters.

In a previous study, Evans et al. [14] utilized a 1D diffusion-reaction

^{*} Corresponding author. Department of Physics and Astronomy, University of Missouri, Columbia, MO, 65211, USA.

^{**} Corresponding author. Division of Plant Science and Technology, College of Agriculture, Food and Natural Resources and Interdisciplinary Plant Group, Christopher S. Bond Life Sciences Center, University of Missouri, 1201 Rollins St, Columbia, MO, 65211, USA.

E mail addresses: yzbn4@mail.missouri.edu (Y. Zhou), yfichman@tauex.tau.ac.il (Y. Fichman), szc5c@mail.missouri.edu (S. Zhang), mittlerr@missouri.edu (R. Mittler), chenshi@missouri.edu (S.-J. Chen).

model to investigate the propagation of the ROS-assisted calcium wave in the root of *Arabidopsis thaliana*. The model employed by the authors simplifies the system as a one-dimensional array of cells, with the NADPH oxidase AtrBOHD (*Arabidopsis thaliana* respiratory burst oxidase homolog D) localized to the plasma membrane. The underlying assumption of their model was based on a self-propagation mechanism, where ROS generated by one RBOHD indirectly activates neighboring RBOHD by triggering an influx of calcium ions through the plasma membrane into the cell. Consequently, the generated ROS can travel through the apoplast, leading to a self-propagating wave along the one-dimensional array of cells. Their findings suggest that the mechanism of RIRR is crucial for the observed transmission velocity of the calcium wave.

Despite the successful modeling of the ROS-mediated calcium wave propagation in the root of *Arabidopsis thaliana*, the model cannot be directly applied to describe the wave velocity of ROS signaling in unicellular communities. Here, we propose a reaction-diffusion model designed to treat microorganism communities rather than plants, taking into account factors such as cell distributions, which can be influenced by both population density and cell mobility. Furthermore, the model explicitly incorporates a cell-density-dependent ROS production/scavenging system to effectively reproduce the experimentally observed wave velocity-population density relationship within colonies of *Chlamydomonas reinhardtii* grown on agar plates. Our model offers therefore insights into the complex interplay between ROS production, cell distribution, and ROS scavenging effects in unicellular communities.

2. Results and discussion

2.1. Measuring the ROS wave in communities of C. reinhardtii at different dilutions

We previously reported that the ROS wave was induced by a local treatment of high light or heat stress in communities of *C. reinhardtii* grown on agar plates [12]. We also reported that accumulation of ROS, and/or the induction of the ROS wave, did not occur if these communities were composed of the Rbo mutant of C. reinhardtii (deficient in the C. reinhardtii homolog of the plant "respiratory burst oxidase homolog" RBOH/NADPH oxidase/NOX [12]). As the RBOH-driven mechanism of the ROS wave in C. reinhardtii requires further analysis, we developed a model for the ROS wave in unicellular organisms based on our previous studies and used computational tools to dissect it. To obtain ROS wave velocities in communities of C. reinhardtii, we grew C. reinhardtii cells on agar plates at different dilutions and measured the propagation velocity of the ROS wave in response to a localized high light stress treatment (Fig. 1A). The high light stress was applied to a local area of the plate using a fiber optic (solid circle in Fig. 1A), and ROS accumulation was measured using H₂DCFDA as described in (Fichman et al. [12]). The intensity of the ROS signal at the local area (solid circle; Fig. 1A) and at an area away from it (systemic area; dashed circle in Fig. 1A) was measured over time (Fig. 1B). From these values, the ROS wave velocity at different dilutions was calculated (Fig. 1C). Based on experimental image snapshots obtained from the varying dilutions, we mapped the areas covered by C. reinhardtii as green and the uncovered areas as white, respectively (Fig. 1D). Subsequently, we estimated the ratio between the area covered by colonies and the total area of the snapshot image by counting pixels. The average estimated ratios (i.e., colony coverage) were 0.1126 \pm 0.0226, 0.2283 \pm 0.0601, and 0.9276 \pm 0.0361 for OD values of 0.012, 0.12, and 1.2, respectively. These estimations were based on five experimental snapshot images taken at each OD value. A plot of the experimentally observed ROS wave velocity ν versus colony coverage ρ is shown in Fig. 1E.

Interestingly, the denser the *C. reinhardtii* community was, the slower was the velocity of the ROS wave (Fig. 1C). This effect could be explained by the scavenging effect of cells (i.e., the capacity of the cytosol to scavenge $\rm H_2O_2$ once it enters it, coupled with the higher overall volume of cytosol found in denser cultures), and/or by the presence of extracellular ROS scavenging metabolites/enzymes found at

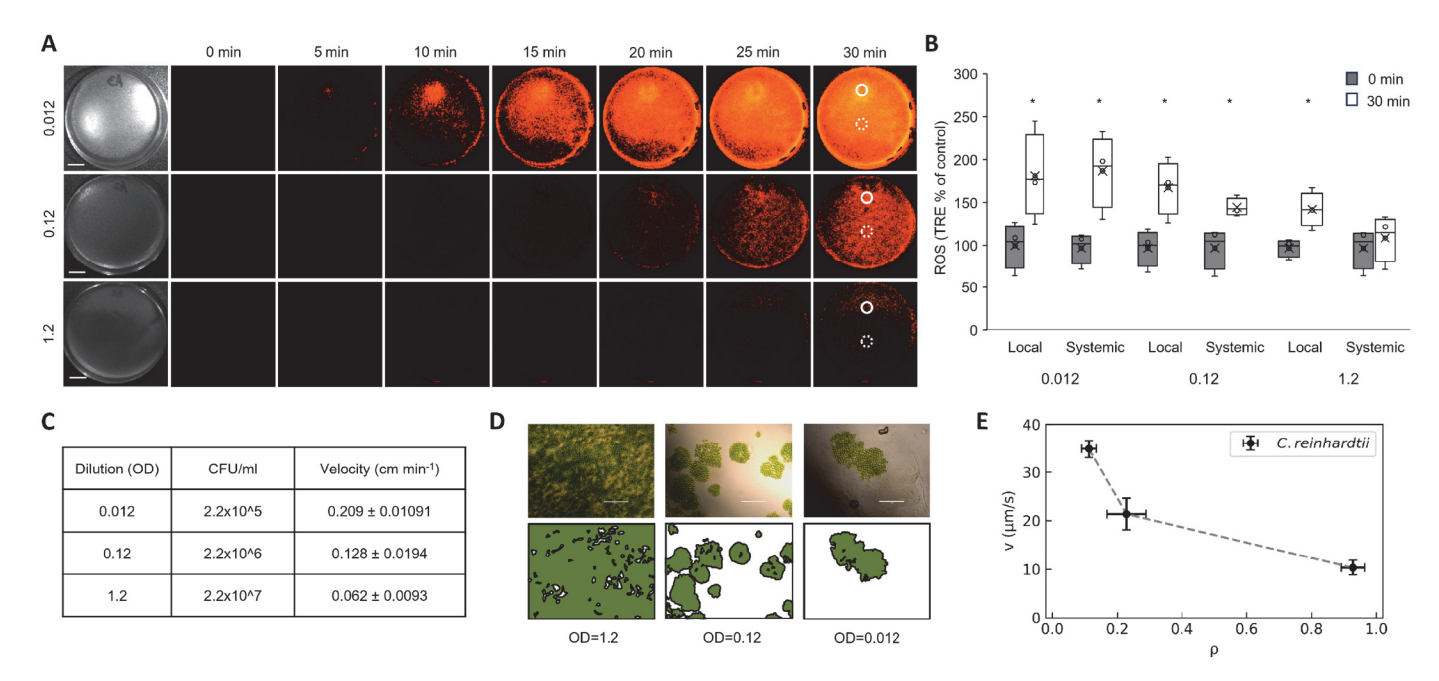


Fig. 1. Measurements of the ROS wave in communities of *C. reinhardtii* cells grown as a lawn on agar plates at different dilutions. (A) Representative time-lapse images showing ROS accumulation in agar plates containing lawns of *C. reinhardtii* cells prepared at dilutions of 1.2, 0.12, and 0.012 OD and treated with a focused beam of high light (local treatment; solid circles). (B) Quantification of local (solid circles) and systemic (dashed circles) ROS levels at 0 and 30 min post-treatment across different cell densities. Data shown as box plot graphs; X is mean \pm S.E., N = 30, *P < 0.05, Student t-test. Scale bar, 1 cm. (C) Table of experimentally measured ROS wave velocities at each dilutions. All experiments were repeated at least 3 times with 10 agar plates per experiment. (D) Representative snapshots of experimentally observed *C. reinhardtii* distributions. Top row depicts experimental image snapshots with OD values of 1.2, 0.12, and 0.012 (left to right), bottom row corresponds to the color-mapped snapshots used for estimating the colony coverage *ρ* via pixel counting. Scale bar, 100 μm. (E) Plot showing experimentally observed ROS wave velocity *ν* versus colony coverage. Abbreviations: OD, optical density; TRE, total radiant efficiency; CFU, colony forming unit.

the extracellular medium of denser cultures (an outcome of secreted antioxidants to the extracellular matrix by cells in denser cultures). In this respect, it should be noted that early work found that the denser a bacterial community was, the higher was its ability to scavenge H2O2 (Ma and Eaton [37]). The process of peroxisome proliferation in the cytosol of plant cells during stress could also have a similar scavenging effect on H2O2 as peroxisomes are rich in the H2O2 scavenging enzyme catalase, and the more peroxisomes are present in the cytosol (following their proliferation) the higher is their ability to scavenge H2O2 that diffuses into them (del Río et al. [38]). Taking into account the high capacity of C. reinhardtii cells to scavenge H₂O₂ (e.g., Dayer et al. [39]), it appears likely that the observed effect of the community density on the velocity of the ROS wave (Fig. 1C) is a direct outcome of H2O2 scavenging by cells, that slows down the propagation of the ROS wave. In future studies it would be interesting to test the velocities of the ROS wave in C. reinhardtii communities that are deficient in cytosolic scavenging capacity of H2O2. At least in plants, it was previously found that the velocity of the ROS wave was faster in mutant plants that lacked the major H₂O₂ scavenging enzyme ascorbate peroxidase 1 (Fichman et al. [40]), supporting this possibility.

2.2. Capturing ROS diffusive dynamics using a continuum reactiondiffusion model with RIRR

In principle, the observed ROS waves in *C. reinhardtii* communities can be explained by the close interplay between ROS production, uptake, and scavenging (Fig. 2A). The driving force behind the ROS wave propagation is the RIRR process (Fig. 2B; red arrows). In this process, ROS produced by activated NADPH oxidases (NOXs) can diffuse into the intercellular space, or spread along the cell surface, triggering enhanced ROS production by activating neighboring NOXs on the same or adjacent cells. Additionally, extracellular ROS (Fig. 2B; blue arrows) originating from adjacent NOXs or the intercellular space can be transported into the cell through aquaporin channels. Moreover, cells also possess effective cytoplasmic scavenging mechanisms (Fig. 2B; green arrows) to maintain balanced intra- and extracellular ROS levels.

We here model the system through a continuum model based on the following reaction-diffusion function:

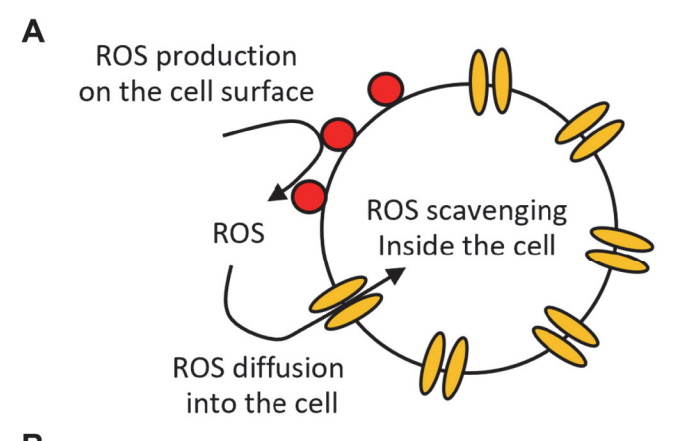
$$\frac{\partial u}{\partial t} = D\nabla^2 u + \alpha \rho H(u - u_{th}) - \gamma \rho u, \tag{1}$$

where u and D are ROS concentration and ROS signal diffusion coefficient, respectively. The effective production and scavenging of ROS by the *C. reinhardtii* are modeled by $\alpha \rho H(u-u_{th})$ and $\gamma \rho u$, respectively, where α and γ are the effective ROS production and scavenging rates and $H(u-u_{th})$ is the Heaviside step function. The production term is proportional to the colony coverage ρ and as shown by the step function $H(u-u_{th})$, is only activated when the local ROS concentration surpasses a specified firing threshold u_{th} . The major feature that differentiates our model from previous studies [14,33,34] is the cell-density-dependent production and scavenging rates. In other words, α and γ are both functions of the colony coverage ρ in our proposed continuum model. This assumption (i.e., cell-density-dependent rates) is based on the experimental observation of cell-density-dependent ROS levels found in cultured neural precursor cells [41] and C. reinhardtii grown on agar plates (this study). For both systems, cells cultured at lower density showed a significantly higher ROS level than the same cells cultured at higher density. Mathematically, we employ the following functional forms for α and γ :

$$\alpha = c + be^{-a\rho}, \gamma = d\rho, \tag{2}$$

where a,b,c, and d are constants to be determined. By rescaling the ROS concentration u and the ROS production rate α by the threshold concentration u_{th} : $u \equiv u/u_{th}$ and $\alpha \equiv \alpha/u_{th}$, we can effectively set u_{th} to 1.

To reveal the relationship between ROS wave velocity and colony



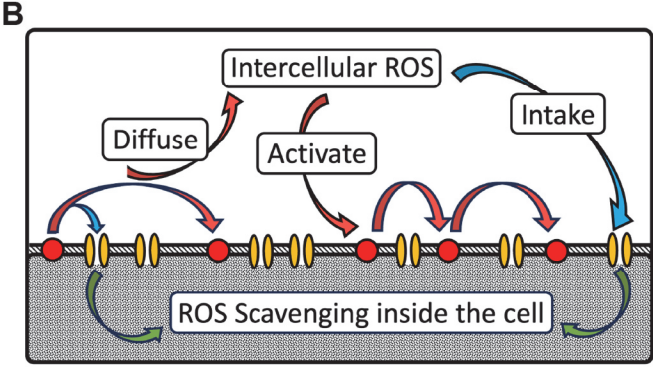




Fig. 2. The conceptual model illustrating the mechanisms underlying the ROS wave propagation. (A) The three key processes within a single *C. reinhardtii* cell. (B) A simplified model for the RIRR signaling pathway. The ROS produced by NOXs (red circles) undergo three paths: (1) The produced ROS can diffuse along or away from the cell surface, activating ROS-producing NOXs in the same or adjacent cells (red arrows); (2) The diffused ROS can be transported into the cell (blue arrows) through aquaporin channels (yellow ellipses); (3) The transported ROS can be scavenged (green arrows) inside the cell (cytoplasm; grey). The interplay between ROS production, transport, and scavenging gives rise to the self-propagating ROS waves observed in algal communities. Not shown is the potential scavenging of ROS outside of cells.

coverage, we focus on the traveling wave solution to the diffusion-reaction equation: $u(r,t)=u(\xi)$ and $\xi=r-vt$ [33], where r is the radial distance and v is the ROS wave speed. In terms of variable ξ , Eq. (1), the original partial differential equation (PDE), is reduced to the following ordinary differential equation (ODE):

$$D\frac{\partial^{2} u}{\partial \xi^{2}} + v\frac{\partial u}{\partial \xi} + \alpha \rho H(-\xi) - \gamma \rho u = 0, \tag{3}$$

where we have omitted the terms $\sim 1/r$ or $1/r^2$ as we are concerned with the asymptotic wave behavior, where the ROS wave front has propagated to a position distant $r\gg D/\nu$ from the initiation spot. Here we also assume the wave is isotropic over θ thus $\partial^2 u/\partial\theta^2\sim 0$. The step function $H(-\xi)$ implies $u(0)=u_{th}$, meaning $\xi=0$ is defined as the wave front where the local ROS concentration equals the firing threshold u_{th} . The above equation can be solved with the conditions $u(0)=u_{th}$ and $\lim_{\xi\to 0^-}u(\xi)=\lim_{\xi\to 0^+}u(\xi)$:

$$u(\xi) = \begin{cases} u_{th}e^{\xi\lambda_{-}}, \xi \ge 0\\ (u_{th} - \alpha/\gamma)e^{\xi\lambda_{+}} + \alpha/\gamma, \xi \le 0, \end{cases}$$
(4)

where $\lambda_{\pm}=\left(-\ \nu\pm\sqrt{
u^2+4D\gamma\rho}\,\right)\!/2D.$ Using the boundary condition

 $\lim_{\xi\to 0^-}\partial u/\partial\xi=\lim_{\xi\to 0^+}\partial u/\partial\xi$ we can derive the ROS wave velocity ν as a function of the model parameters:

$$v = \left\{ 4D\gamma \rho \left[\left(1 - \frac{2\gamma u_{th}}{\alpha} \right)^{-2} - 1 \right]^{-1} \right\}^{1/2}$$

$$= \left\{ 4Dd\rho^2 \left[\left(1 - \frac{2d\rho}{c + be^{-a\rho}} \right)^{-2} - 1 \right]^{-1} \right\}^{1/2}.$$
(5)

The model involves five parameters (D, a, b, c, and d). Based on the experimentally observed H₂O₂ diffusion coefficient [42,43], we set the diffusion coefficient D to be 1000 $\mu m^2/s$. From the decay constant k of H_2O_2 observed in 0.2 % agarose slices [43], we set the decay rate d to be 0.1 s^{-1} . By combining Eq. (5) and the experimental data (Fig. 1) for the ROS velocity for the different colony coverages, we find the effective parameters: a = 14, b = 50 and c = 0.35. As shown in Fig. 3, using the cell-density-dependent production α and scavenging γ rates (Fig. 3B), the model recapitulates the observed wave velocity-colony coverage relationship (Fig. 3A). The ROS concentration profiles at the traveling wave front ($\xi = 0$) for different colony coverages exhibit an exponential decay in the (non-excited) region $\xi > 0$ where the ROS concentration *u* is below the threshold u_{th} for the excitation of ROS (Fig. 3C). To investigate the general behavior of ROS wave propagation, we also performed simulations to solve Eq. (1) without the traveling wave ansatz in polar coordinates for $\rho = 0.9276$. As shown in Fig. 3D, the ROS velocity calculated from the simulated ROS concentration profiles at different timestamps closely reproduces the observed result. The result supports the validity of the analytical solution with the traveling wave ansatz. See Materials and Methods for descriptions of the parameters and variables and technical details of the simulation.

2.3. Simulating ROS diffusive dynamics with sampled colony distributions

To further validate the continuum model and the associated model parameters, we went beyond the continuum model by sampling discrete colony distributions that resemble the actual distribution observed in experiments. Specifically, we modified Eq. (1) to incorporate the sampled discrete colony distributions:

$$\frac{\partial u}{\partial r} = D\nabla^2 u + \alpha \varphi(r)H(u - u_{th}) - \gamma \varphi(r)u, \tag{6}$$

where the colony coverage $ho({\pmb r}) \equiv \varphi({\pmb r})$ now depends on the position ${\pmb r}$:

$$\varphi(\mathbf{r}) = \begin{cases} 0, \mathbf{r} \text{ outside colony} \\ 1, \mathbf{r} \text{ inside colony.} \end{cases}$$
 (7)

Here, we use $\varphi(r)$ to represent the position-dependent colony coverage $\rho(r)$ in order to distinguish it from the average colony coverage ρ used in the previous sections.

Sampling experimentally observed G. reinhardtii colony distributions on agar plates. The average colony coverage ρ can be estimated from experimental snapshots of colony distributions (Figs. 1D and 4). To sample discrete colony distributions (i.e., $\varphi(\mathbf{r})$) for a given colony coverage (from OD), we employed a progressive sampling procedure. In this procedure, G. reinhardtii colonies with diameters following a Gaussian distribution $\mathcal{N}(\mu, \sigma^2)$ are repeatedly placed until the colony coverage ρ , representing the occupied area ratio, reaches the aforementioned threshold value. Overlapped regions between colonies are

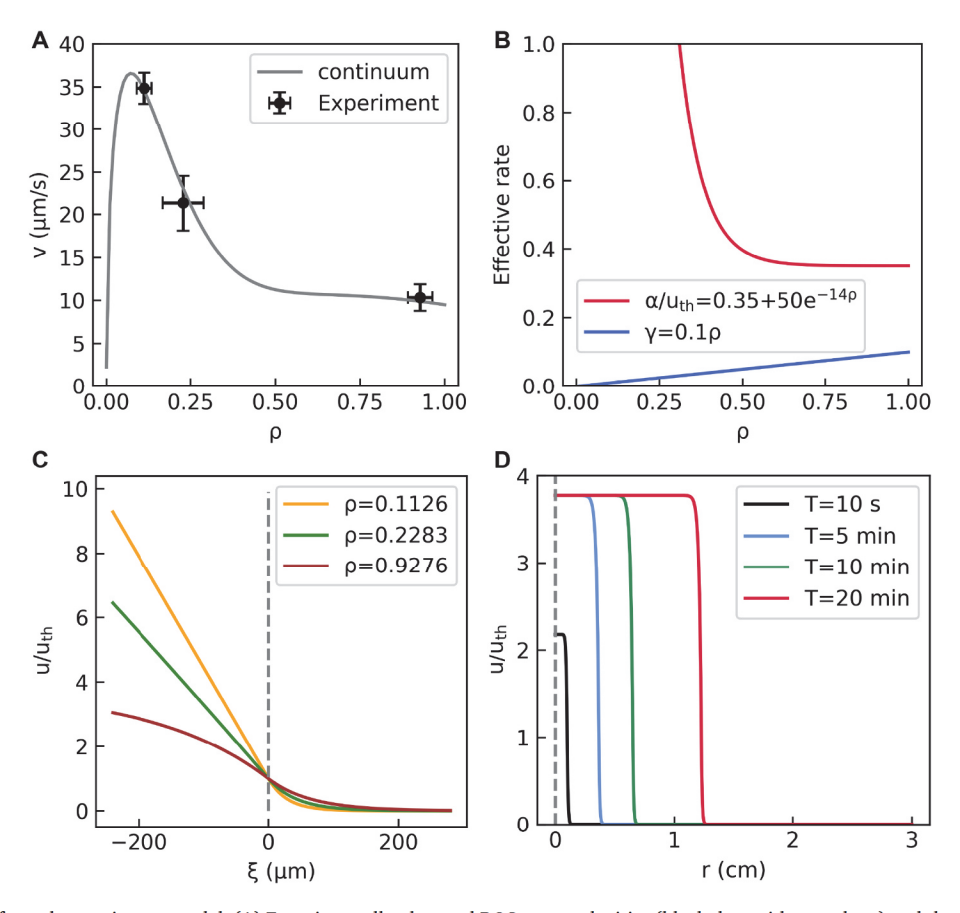


Fig. 3. Results obtained from the continuum model. (A) Experimentally observed ROS wave velocities (black dots with error bars) and the calculated wave velocity-colony coverage $(\nu-\rho)$ curve (grey). (B) The fitted α and γ functions used for deriving velocities in (A). (C) ROS wave front concentration profiles over ξ for different colony coverages. (D) Simulated ROS concentration profiles for a particular colony coverage ($\rho=0.9276$) at different timestamps. The initial activation area is centered at the origin with a radius of 1 mm.

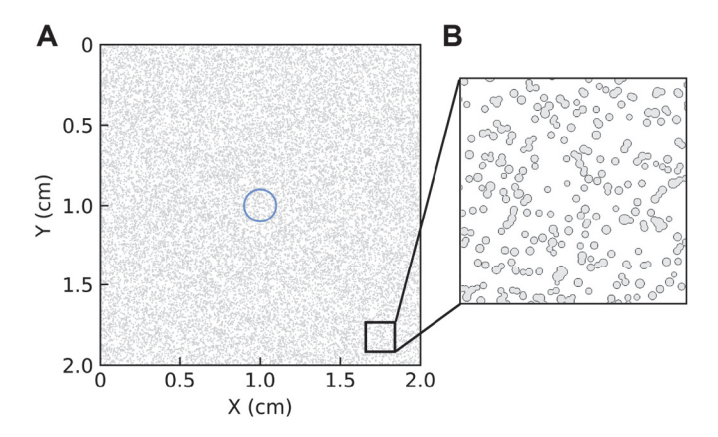


Fig. 4. Example snapshots of computationally sampled *C. reinhardtii* distributions. (A) Illustration of the sampled *C. reinhardtii* distribution that satisfies the ratio threshold for an OD value of 0.12 (i.e., $\rho=0.2283$). Blue circle encloses the stimulated area with a radius of 1 mm. 23,062 pseudo colonies are confined in a virtual 2D square plate with a size of 2 \times 2 cm. Each colony in the plate is characterized by a circle with diameter randomly sampled from the Gaussian distribution with mean μ and standard deviation σ set to 75 μm and 10 μm , respectively. (B) A zoomed-in view of a 2 \times 2 cm sampled colony distributions (colonies are shown in grey color).

only counted once. In the specific case shown in Fig. 4, the colony coverage ρ is set to 0.2283, and from the experimental snapshots, we estimated the colony size distribution with the mean diameter μ and the standard deviation σ : $\mu \simeq 75~\mu m$ and $\sigma \simeq 10~\mu m$.

Reproducing observed ROS wave velocities for sampled C. reinhardtii colony distributions on agar plates. The technical details of the simulation can be found in the Materials and Methods. There are three types of ROS wave velocities calculated for each simulation: v_{fast} , v_{slow} , and v_{avg} . v_{fast} and v_{slow} were calculated by $v_{fast} = (R_{max}(t) - R_0)/t$ and $v_{slow} =$ $(R_{\it min}(t) - R_0)/t$, where $R_{\it max}(t)$ and $R_{\it min}(t)$ represent the farthest and nearest propagated distances from the origin during the stimulation time t, and R_0 is the radius of the initially stimulated area. v_{avg} is the average ROS wave velocity calculated from $u_{
m avg} \, = \left(\sqrt{A/\pi} \, - R_0 \right)\!/\,t$, where A is the area of the plate with ROS concentration exceeding the firing threshold and $\sqrt{A/\pi}$ is the effective radius of coverage of the excited area. See Fig. 5A-F for snapshots of ROS wave propagation from the initially stimulated area at different timestamps. The ROS wave velocities obtained from the simulations were plotted against time (Fig. 5G-I), and the results indicate that the simulated v_{fast} can closely reproduce the experimentally observed ROS wave velocities for different colony distributions. The larger discrepancy between the v_{avg} and the observed wave velocity for systems of low colony density (Fig. 5G) is expected, as the system largely deviates from the continuum limit.

3. Conclusions and future development

Transmission of RIRR signals is a general principle in biology used to propagate information in the form of 'altered ROS production state' between different subcellular compartments/organelles, cells, tissues, and even different organisms [9,11,12]. We have recently shown that this signaling mechanism functions in communities of microorganisms such as *Chlamydomonas reinhardtii* and *Dictyostelium discoideum* grown on agar plates [12]. Here, we applied a reaction-diffusion model with RIRR to explore the mechanisms behind the systemic transmission of stress-induced ROS waves in communities of *C. reinhardtii* grown on the surface of an agar plate. In this respect, it should be noted that in nature *C. reinhardtii* was found to grow on soil, snow, and other surfaces [44, 45]. Our analyses suggest that the reaction-diffusion model with RIRR is able to reproduce the observed ROS transmission velocity in unicellular microorganism communities of *C. reinhardtii* grown on agar plate. With

the manipulation of key parameters (e.g., D, α , and γ), our model can be applied to systems under various conditions (e.g., different ROS scavenger/inhibitors, mixed cell populations, and wild type/mutant cell mixtures [12]). In addition, as our model takes into consideration the interplay between production and scavenging ROS rates, it could be adapted to explain RIRR signaling pathways in many other systems and organisms, as well as in microbiomes that play a key role in our ecosystems (e.g., Refs. [12,13]). Future development of our model should include: (1) Consideration of the scavenging effect within the intercellular space. We can also consider the scavenging effect in intercellular spaces in the presence or absence of different concentrations of various ROS scavengers, including information of the reaction types between different scavengers and ROS. (2) Accounting for the 3D nature of cells. While the cells modeled here were cultured on the 2D surface of the plate, the cells are 3D objects and can even form layers, depending on the population density. For example, unicellular algae have been observed to move/vibrate in an up/down fashion. This certainly adds 3D aspects to the ROS signal transmission in space. To investigate the effects of the extra dimension on the ROS signal propagation, we can extend the model to 3D by modeling the cells as 3D objects of a given size and shape. In future studies, we can also adapt the approach developed for 2D cell distributions, expanding the sampling space of cell distributions and extending the diffusion-reaction equation to 3D space. (3) Modeling the effect of cell mobility on ROS signal transmission. Unicellular organism such as C. reinhardtii and amoeba, growing in liquid, or mixed solid/liquid media, may exhibit mobility (e.g., chemo- and photo-taxis) during the experiment, such system will be drastically different from the static ones, and our current model may not be able to capture the dynamics and require further modifications. A potential solution is to consider the movement of cells and the propagation of ROS signals as two distinct and independent events. By treating cells as beads, we can use the Brownian dynamic to simulate the trajectory of each individual cell within the community, then we can explicitly incorporate the movement of each cell in the simulations with the proposed reaction-diffusion model. Another modification that might be needed in the future is the consideration of other ROS species produced by, for example, the chloroplast, mitochondria, or peroxisomes. In the current study we developed a model for NADPH oxidase-driven ROS (that is based on the finding that ROS accumulation detected in our experimental assay is fully dependent on the Rbo gene of C. reinhardtii [12]. However, other types of ROS could contribute to the ROS wave. The analysis of these other types of ROS may require further modifications of the model. In future studies the scavenging potential of different communities with different densities should also be measured. This will require however the development of ROS imaging systems for cells grown in liquid, and proper antioxidant assays. As ROS and redox play such a central role in biology [46-50], developing tools and methods to study ROS/redox signaling is one of the highest priorities for biological research. As described above, the newly developed model described in this work could be further developed and/or used to explain RIRR signaling mechanisms common to many different biological processes and systems occurring in different organisms, required for our health as well as the health of our ecosystems.

4. Materials and Methods

Organism. Chlamydomonas reinhardtii cells were obtained from the Chlamydomonas Resource Center, University of Minnesota, St. Paul, MN, USA, and the UTEX Culture Collection of Algae, Austin, TX, USA. C. reinhardtii cultures were grown on agar plates containing P49 solid media (UTEX Culture Collection of Algae, Austin, TX, USA) as described in Fichman et al. [12]. Cultures in different dilutions were grown for 3 days at 8 h/16 h light/dark cycles before ROS imaging.

ROS imaging. Agar plates containing culture (lawns) of C. reinhardtii cells, prepared at different dilutions, were fumigated with 50 μ M H_2 DCFDA (Ex./Em. 480 nm/520 nm; Millipore-Sigma, St. Louis, MO,

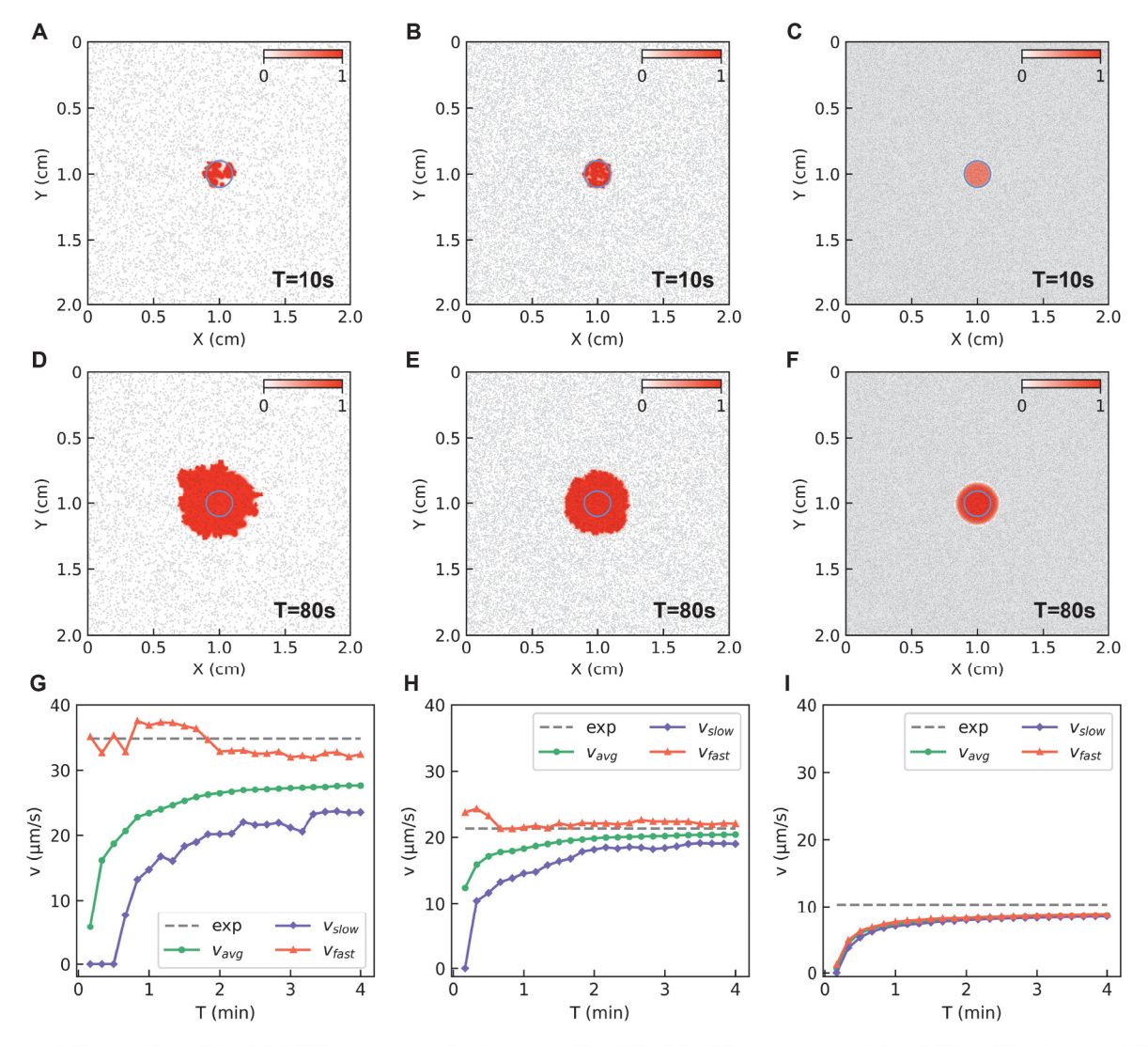


Fig. 5. Representative snapshots of simulated ROS wave propagation in communities of C. reinhardtii grown on agar plates at different timestamps and the derived ROS wave velocities for different colony coverages (A,D,G) $\rho=0.1126$, (B,E,H) $\rho=0.2283$, and (C,F,I) $\rho=0.9276$. (A–F) Snapshots of the simulated ROS concentration distributions at different timestamps. (A–C) At the beginning of the simulation (T = 10 s), ROS are still confined within the initially stimulated region (blue circle with a radius of 1 mm). (D–F) ROS concentration distributions after simulating the entire system for 80 s. The color bar represents the relative strength of the ROS signal (i.e., ROS concentration), where a higher concentration of ROS is depicted by a redder color. (G–I) Calculated ROS wave velocities at different timestamps. The dashed lines (grey) represent the experimentally measured wave velocities. The model parameters obtained from the continuum model are employed for the simulation. The systems were simulated with time step of 10^{-3} s, grid size of 5 μ m, and no-flux boundary conditions on the boundary of the (square) system. See Materials and Methods for an explanation of the parameters and variables and technical details of the simulations.

USA) in 0.05 M Phosphate buffer pH 7.4 with 0.01 % Silwet L-77. Fumigation was carried out for 30 min using nebulizers (Punasi Direct, Hong Kong, China). Following H_2DCFDA fumigation, high light stress (1500 µmole photons $m^{-2}s^{-1}$) was applied with a fiber optic light source for 2 min as described in Fichman et al. [12] and live ROS accumulation was imaged using the IVIS Lumina S5 platform (Fichman et al. [12,40]). Acquired images were then analyzed using the math function in Living Image software (PerkinElmer, Waltham, MA, USA), and graphs generated as described in Fichman et al. [12].

Finite difference method for simulating the continuum model. Using polar coordinates, the continuum model can be written as the following:

$$\frac{\partial u}{\partial t} = D \frac{\partial^2 u}{\partial r^2} + \frac{D}{r} \frac{\partial u}{\partial r} + \frac{D}{r^2} \frac{\partial^2 u}{\partial \theta^2} + \alpha \rho H(u - u_{th}) - \gamma \rho u. \tag{8}$$

We can discretize the simulated system over the polar radius r and the time t, and denote $u_i^k \equiv u(r_i, t_k)$. Using the FTCS (forward time-

centered space) method, we can explicitly write the recurrence equation:

$$\begin{split} u_{i}^{k+1} &= \alpha \rho \Delta t H(u - u_{th}) + (1 - \gamma \rho \Delta t) u_{i}^{k} + \frac{D \Delta t}{(\Delta r)^{2}} \left(u_{i+1}^{k} + u_{i-1}^{k} - 2 u_{i}^{k} \right) \\ &+ \frac{D \Delta t}{2r \cdot \Delta r} \left(u_{i+1}^{k} + u_{i-1}^{k} \right), \end{split} \tag{9}$$

where Δr and Δt are the one-dimensional bin size and the time step size, respectively. The simulated system size (radius) is 3 cm, and the initial activated area is centered at the origin with a radius of 1 mm. The bin and time step sizes are set to 10 μ m and 0.0001 s, respectively. No-flux boundary conditions (i.e., $\partial u/\partial n|_{boundary}=0$) are implemented at the system boundaries.

Finite difference method for simulating the model on sampled colony distribution. Using Cartesian coordinates, the model can be written as the following:

$$\frac{\partial u}{\partial t} = D \left[\frac{\partial^2 u}{\partial x^2} + \frac{\partial^2 u}{\partial y^2} \right] + \alpha \varphi(\mathbf{r}) H(u - u_{th}) - \gamma \varphi(\mathbf{r}) u. \tag{10}$$

We can discretize the simulated system over the Cartesian coordinates (x and y) and the time t, and denote $u_{i,j}^k \equiv u(x_i, y_j, t_k)$. Using the FTCS (forward time-centered space) method, we can explicitly write the recurrence equation:

$$\begin{split} u_{i,j}^{k+1} &= \alpha \varphi(\mathbf{r}) \Delta t H(u - u_{th}) + (1 - \gamma \varphi(\mathbf{r}) \Delta t) u_{i,j}^k + \frac{D \Delta t}{\left(\Delta t\right)^2} \left(u_{t+1,j}^k + u_{t-1,j}^k + u_{t,j+1}^k + u_{t,j-1}^k - 4 u_{i,j}^k \right), \end{split} \tag{11}$$

where Δl and Δt are the bin size (same for x and y) and the time step size, respectively. The dimension of the simulated system size is 2×2 cm, and the initial activated area is centered at the origin with a radius of 1 mm. The bin size and the time step size are set to 5 μm and 0.001 s, respectively. No-flux boundary conditions (i.e., $\partial u/\partial n|_{boundary}=0$) are implemented at the system boundaries.

Funding

This work was supported by the National Institutes of Health under Grant R35-GM134919 to S-J. C. and National Science Foundation under Grants IOS-1932639 and IOS-2343815 to R. M.

Data availability statement

The data supporting the findings of this study are available in the manuscript or in the supplementary materials.

Declaration of generative AI in scientific writing

The large language model (LLM), Claude, developed by Anthropic was used for language refinement only.

CRediT authorship contribution statement

Yuanzhe Zhou: Writing - original draft, Methodology, Investigation. Yosef Fichman: Writing - review & editing, Investigation, Data curation. Sicheng Zhang: Writing - original draft, Investigation. Ron Mittler: Writing – review & editing, Supervision, Funding acquisition, Conceptualization. Shi-Jie Chen: Writing - review & editing, Supervision, Funding acquisition, Conceptualization.

Declaration of competing interest

The authors declare that they have no known competing financial interests or personal relationships that could have appeared to influence the work reported in this paper.

Details of parameters and variables

Name Description

u(r,t)ROS concentration at radial distance r and time t since stimulation

ROS threshold concentration for activating ROS production u_{th}

ratio between C. reinhardtii covered area and plate's area

discrete colony distribution at position r $\varphi(\mathbf{r})$

D ROS signal diffusion coefficient

effective ROS production rate α

effective ROS scavenging rate γ

radial distance to the center of the stimulation

t time interval since the stimulation

traveling wave speed of the ROS wave ν

ξ transformed radial distance in the traveling wave frame of reference

mean of the Gaussian distribution used to sample colony μ

standard deviation of the Gaussian distribution used to sample colony

References

- [1] Jeremy B. Chang, James E. Ferrell Jr., Mitotic trigger waves and the spatial coordination of the xenopus cell cycle, Nature 500 (7464) (2013) 603-607.
- [2] Lendert Gelens, Graham A. Anderson, James E. Ferrell Jr., Spatial trigger waves: positive feedback gets you a long way, Mol. Biol. Cell 25 (22) (2014) 3486–3493. PMID: 25368427.
- [3] Xianrui Cheng, James E. Ferrell Jr., Apoptosis propagates through the cytoplasm as trigger waves, Science 361 (6402) (2018) 607-612.
- [4] Eduardo Reátegui, Fatemeh Jalali, Aimal H. Khankhel, Elisabeth Wong Hansang Cho, Jarone Lee, Charles N. Serhan, Jesmond Dalli, Hunter Elliott, Daniel Irimia, Microscale arrays for the profiling of start and stop signals coordinating human-neutrophil swarming, Nat. Biomed. Eng. 1 (7) (2017) 94.
- [5] Gad Miller, Karen Schlauch, Rachel Tam, Diego Cortes, Miguel A. Torres, Vladimir Shulaev, Jeffery L. Dangl, Ron Mittler, The plant nadph oxidase rbohd mediates rapid systemic signaling in response to diverse stimuli, Sci. Signal. 2 (84)
- Aaron Baxter, Ron Mittler, Nobuhiro Suzuki, ROS as key players in plant stress signalling, J. Exp. Bot. 65 (5) (2013) 1229–1240.
- Won-Gyu Choi, Gad Miller, Ian Wallace, Jeffrey Harper, Ron Mittler, Simon Gilroy, Orchestrating rapid long-distance signaling in plants with ca2+, ros and electrical signals, Plant J. 90 (4) (2017) 698-707.
- [8] Cezary Waszczak, Melanie Carmody, Jaakko Kangasjärvi, Reactive oxygen species in plant signaling, Annu. Rev. Plant Biol. 69 (1) (2018) 209-236. PMID: 29489394.

- [9] Sara I. Zandalinas, Ron Mittler, Ros-induced ros release in plant and animal cells, Free Radic, Biol. Med. 122 (2018) 21-27.
- [10] Yosef Fichman, Ron Mittler, Rapid systemic signaling during abiotic and biotic stresses: is the ros wave master of all trades? Plant J. 102 (5) (2020) 887-896.
- [11] Ron Mittler, Sara I. Zandalinas, Yosef Fichman, Frank Van Breusegem, Reactive oxygen species signalling in plant stress responses, Nat. Rev. Mol. Cell Biol. 23 (10)
- [12] Yosef Fichman, Linda Rowland, Melvin J. Oliver, Ron Mittler, Ros are evolutionary conserved cell-to-cell stress signals, Proc. Natl. Acad. Sci. USA 120 (31) (2023)
- [13] Yosef Fichman, Linda Rowland, Thi Thao Nguyen, Shi-Jie Chen, Ron Mittler, Propagation of a rapid cell-to-cell h2o2 signal over long distances in a monolayer of cardiomyocyte cells, Redox Biol. 70 (2024) 103069.
- [14] Matthew J. Evans, Won-Gyu Choi, Simon Gilroy, Richard J. Morris, A ROS-assisted calcium wave dependent on the AtRBOHD NADPH oxidase and TPC1 cation channel propagates the systemic response to salt stress, Plant Physiol. 171 (3) (2016) 1771-1784.
- [15] David A. Kessler, Herbert Levine, Pattern formation in dictyostelium via the dynamics of cooperative biological entities, Phys. Rev. E 48 (1993) 4801-4804.
- [16] Javad Noorbakhsh, David J. Schwab, Allyson E. Sgro, Thomas Gregor, Pankaj Mehta, Modeling oscillations and spiral waves in dictyostelium populations, Phys. Rev. E 91 (2015) 062711.
- Shigeru Kondo, Takashi Miura, Reaction-diffusion model as a framework for understanding biological pattern formation, Science 329 (5999) (2010) 1616-1620.

- [18] Eiríkur Pálsson, Edward C. Cox, Origin and evolution of circular waves and spirals in Dictyostelium discoideum territories, Proc. Natl. Acad. Sci. USA 93 (3) (1996) 1151–1155
- [19] Judith Pérez-Velázquez, Meltem Gölgeli, Rodolfo García-Contreras, Mathematical modelling of bacterial quorum sensing: a review, Bull. Math. Biol. 78 (8) (2016) 1585–1639.
- [20] Herman J. Eberl, David F. Parker, Mark C.M. Vanloosdrecht, A new deterministic spatio-temporal continuum model for biofilm development, J. Theor. Med. 3 (3) (2001) 161–175.
- [21] Benjamin L. Vaughan Jr., Bryan G. Smith, David L. Chopp, The influence of fluid flow on modeling quorum sensing in bacterial biofilms, Bull. Math. Biol. 72 (5) (2010) 1143–1165.
- [22] Mallory R. Frederick, Christina Kuttler, Burkhard A. Hense, Hermann J. Eberl, A mathematical model of quorum sensing regulated eps production in biofilm communities, Theor. Biol. Med. Model. 8 (1) (2011) 8.
- [23] Lufang Zhou, Miguel A. Aon, Tabish Almas, Sonia Cortassa, Raimond L. Winslow, Brian O'Rourke, A reaction-diffusion model of ros-induced ros release in a mitochondrial network, PLoS Comput. Biol. 6 (1) (2010) 1–15.
- [24] Ling Yang, Paavo Korge, James N. Weiss, Zhilin Qu, Mitochondrial oscillations and waves in cardiac myocytes: insights from computational models, Biophys. J. 98 (8) (2010) 1428–1438.
- [25] James P. Keener, Propagation of waves in an excitable medium with discrete release sites, SIAM J. Appl. Math. 61 (1) (2000) 317–334.
- [26] Toshihiro Sera, Shingo Komine, Masataka Arai, Yasuhiro Sunaga, Hideo Yokota, Susumu Kudo, Three-dimensional model of intracellular and intercellular ca2+ waves propagation in endothelial cells, Biochem. Biophys. Res. Commun. 505 (3) (2018) 781–786.
- [27] Silvina Ponce Dawson, Joel Keizer, John E. Pearson, Fire-diffuse-fire model of dynamics of intracellular calcium waves, Proc. Natl. Acad. Sci. USA 96 (11) (1999) 6060–6063.
- [28] Stephen Coombes, Robert Hinch, Yulia Timofeeva, Receptors, sparks and waves in a fire-diffuse-fire framework for calcium release, Prog. Biophys. Mol. Biol. 85 (2) (2004) 197–216.
- [29] Joel Keizer, Gregory D. Smith, Silvina Ponce-Dawson, John E. Pearson, Saltatory propagation of ca2+ waves by ca2+ sparks, Biophys. J. 75 (2) (1998) 595–600.
- [30] Yulia Timofeeva, Stephen Coombes, Wave bifurcation and propagation failure in a model of ca2+ release, J. Math. Biol. 47 (3) (2003) 249–269.
- [31] Raz Kupferman, Partha P. Mitra, P.C. Hohenberg, Samuel S.-H. Wang, Analytical calculation of intra-cellular calcium wave characteristics, Biophys. J. 72 (6) (1997) 2430–2444.
- [32] Geneviève Dupont, Laurent Combettes, Gary S. Bird, James W. Putney, Calcium oscillations, Cold Spring Harbor Perspect. Biol. 3 (3) (2011) a004226.
- [33] Paul B. Dieterle, Jiseon Min, Daniel Irimia, Ariel Amir, Dynamics of diffusive cell signaling relays, Elife 9 (2020) e61771.

- [34] Paul B. Dieterle, Ariel Amir, Diffusive wave dynamics beyond the continuum limit, Phys. Rev. E 104 (2021) 014406.
- [35] Elizabeth J. Pereira, Christian M. Smolko, Kevin A. Janes, Computational models of reactive oxygen species as metabolic byproducts and signal-transduction modulators, Front. Pharmacol. 7 (2016) 232070.
- [36] Sonia Cortassa, Miguel A. Aon, Raimond L. Winslow, Brian O'Rourke, A mitochondrial oscillator dependent on reactive oxygen species, Biophys. J. 87 (3) (2004) 2060–2073.
- [37] Muchou Ma, John W. Eaton, Multicellular oxidant defense in unicellular organisms, Proc. Natl. Acad. Sci. USA 89 (17) (1992) 7924–7928.
- [38] Luis A. del Río, Luisa M. Sandalio, Josém. Palma, Pablo Bueno, Francisco J. Corpas, Metabolism of oxygen radicals in peroxisomes and cellular implications, Free Radic. Biol. Med. 13 (5) (1992) 557–580.
- [39] Régine Dayer, Beat B. Fischer, Rik I.L. Eggen, Stéphane D. Lemaire, The peroxiredoxin and glutathione peroxidase families in Chlamydomonas reinhardtii, Genetics 179 (1) (2008) 41–57.
- [40] Yosef Fichman, Gad Miller, Ron Mittler, Whole-plant live imaging of reactive oxygen species, Mol. Plant 12 (9) (2019) 1203–1210.
- [41] Charles L. Limoli, Radoslaw Rola, Erich Giedzinski, Sailaja Mantha, Ting-Ting Huang, John R. Fike, Cell-density-dependent regulation of neural precursor cell function, Proc. Natl. Acad. Sci. USA 101 (45) (2004) 16052–16057.
- [42] Z.C. Liu, D.X. Liu, C. Chen, D. Li, A.J. Yang, M.Z. Rong, H.L. Chen, M.G. Kong, Physico-chemical processes in the indirect interaction between surface air plasma and deionized water, J. Phys. D Appl. Phys. 48 (49) (2015) 495201.
- [43] A. Ledo, E. Fernandes, A. Salvador, J. Laranjinha, R.M. Barbosa, In vivo hydrogen peroxide diffusivity in brain tissue supports volume signaling activity, Redox Biol. 50 (2022) 102250.
- [44] Severin Sasso, Herwig Stibor, Maria Mittag, Arthur R. Grossman, The natural history of model organisms: from molecular manipulation of domesticated Chlamydomonas reinhardtii to survival in nature, Elife 7 (2018) e39233.
- [45] Patrice A. Salomé, Sabeeha S. Merchant, A series of fortunate events: introducing Chlamydomonas as a reference organism, Plant Cell 31 (8) (2019) 1682–1707.
- [46] Magdalena L. Circu, Tak Yee Aw, Reactive oxygen species, cellular redox systems, and apoptosis, Free Radic. Biol. Med. 48 (6) (2010) 749–762.
- [47] Paul D. Ray, Bo-Wen Huang, Yoshiaki Tsuji, Reactive oxygen species (ros) homeostasis and redox regulation in cellular signaling, Cell. Signal. 24 (5) (2012) 981–990.
- [48] Nobuhiro Suzuki, Shai Koussevitzky, Ron Mittler, Gad Miller, Ros and redox signalling in the response of plants to abiotic stress, Plant Cell Environ. 35 (2) (2012) 259–270.
- [49] Michael Schieber, Navdeep S. Chandel, Ros function in redox signaling and oxidative stress, Curr. Biol. 24 (10) (2014) R453–R462.
- [50] Graham Noctor, Jean-Philippe Reichheld, Christine H. Foyer, Ros-related redox regulation and signaling in plants, Semin. Cell Dev. Biol. 80 (2018) 3–12.